ISBN: 978-3-95450-247-9 ISSN: 2673-5490 doi: 10.18429/JACoW-IPAC2024-TUPC81

# CHARACTERIZATION OF RADIATION DAMAGES TO POSITRON SOURCE MATERIALS*

T. Lengler[1,2], K. Aulenbacher[3,4,5], T. Beiser[3,4,5], M. Dehn[3], R. Dorkel[6], M. Formela[2], F. Gauthier[6], B. Geoffroy[6], J. Grames[7], C. Le Galliard[6], S. Habet[6], D. Lott[1], G. Moortgat-Pick[2,8], S. Riemann[9], A. Thiebault[6], A. Ushakov[7], E. Voutier[6], S. Wallon[6]
[1]Helmholtz-Zentrum Hereon, 21502 Geesthacht, Germany
[2]Institut für Theoretische Physik, Universität Hamburg, 22761 Hamburg, Germany
[3]Institut für Kernphysik, Johannes Gutenberg Universität, 55122 Mainz, Germany
[4]HIM, Helmholtz Institüt Mainz, 55128 Mainz, Germany
[5]GSI, Helmholtz-Zentrum für Schwerionenforschung, 64291 Darmstadt, Germany
[6]Université Paris-Saclay, CNRS/IN2P3, IJCLab, 91405 Orsay, France
[7]Thomas Jefferson National Accelerator Facility, Newport News, VA 23606, USA
[8]Deutsches Elektronen-Synchrotron DESY, 22607 Hamburg, Germany
[9]Deutsches Elektronen-Synchrotron DESY, 15738 Zeuthen, Germany



*Abstract*

The production of secondary beams at future positron sources for the Continuous Electron Beam Accelerator Facility (CEBAF), the International Linear Collider (ILC) or the Future Circular Collider (FCC), features unprecedented mechanical and thermal stresses which may compromise sustainable and reliable operation. Candidate materials must possess high melting temperature together with excellent thermal conductivity and radiation hardness. This work reports about the investigation of radiation hardness properties of different materials, performed at the injector of the MAMI (Mainzer Mikrotron) facility and characterized at the HEMS (High Energy Materials Science) beamline operated by the Helmholtz-Zentrum Hereon at the PETRA III synchrotron facility.

## INTRODUCTION

Intense polarized electron and positron beams [1–3] are of substantial importance for the physics reach of future $e^+e^-$ and $e^\pm A$ colliders, as well as for existing fixed target lepton beam facilities. Due to the high luminosity demands the critical issue for all designs is the positron source [4, 5]. At the ILC, a mature baseline design [6] based on an undulator is foreseen for the production of polarized positrons. The E166 experiment [7–9] at the Stanford Linear Accelerator Center successfully demonstrated this technique proposed in Ref. [10]. As alternative an electron-driven unpolarized positron source [11] is discussed. At $Ce^+$BAF [12], a polarized electron-driven source is considered to create polarized positron beams via the so called PEPPo (Polarized Electrons for Polarized Positrons) technique [13] producing polarized positrons from polarized bremsstrahlung radiation induced by a polarized electron beam in a high-$Z$ target. The large amount of required particles (both $e^-$ and $e^+$) is challenging, causing a high load of peak energy deposited density (PEDD) in the target. In the present study different positron sources materials – depending on the primary beam nature ($e^-$ or $\gamma$) and intensity – are analyzed. The modular high-quality electron beam at MAMI generates adjustable and specific PEDDs on the target, comparable for instance to the annual PEDD load expected at ILC. The high thermal stress subsequently produced in the target samples is analyzed via synchrotron diffraction methods at the HEMS beamline.

## MATERIAL IRRADIATION

The MAMI injector LinAc can deliver a 3.5 MeV electron beam of up to 100 $\mu$A in Continuous Wave (CW) mode. The short beam line following the LinAc can be used for a variety of smaller experiments and is ideally suited for irradiation investigations. It is equipped with a vertically movable in-vacuum target holder for different purposes. During previous experiments the beam has been focused to a round spot size of ~50 $\mu$m width at a low beam current of 20 nA using a wire scanner for diagnosis. At higher beam currents the beam size would be significantly larger due to space charge effects. An upper limit ~200 $\mu$m has been determined using an optical transition radiator.

The MAMI electron source can be used in a pulsed mode during normal operation. The peak current is set and measured in CW mode to 50 $\mu$A each time before different pulse schemes are chosen. The average beam current during the irradiation runs was 2.5-11 $\mu$A following the pulse settings.

The material samples are mounted on an aluminum frame which supports up to five samples electrically and thermally isolated with ceramic spacers. Beam diagnostics are mounted on top of the holder with a 45° angle and constitute of an optical transition radiation screen for determination of the beam spot size, and a luminescent screen for beam position control [14]. The whole assembly is attached to a

* This work was supported by the European Union's Horizon 2020 Research and Innovation program under Grant Agreement No 824093, the French Centre National de la Recherche Scientifique, and the U.S. Department of Energy, Office of Science, Office of Nuclear Physics under contract DE-AC05-06OR23177.

ISBN: 978-3-95450-247-9 ISSN: 2673-5490 doi: 10.18429/JACoW-IPAC2024-TUPC81

Table 1: Material Irradiation Specifications

| # | Target $A$ | $t_A$ ($\mu$m) | $w_A$ (mm) | Beam Pulse $\Delta l$ (ms) | $L$ (ms) | Rad. Damage (dpa) | Charge $\delta Q/\delta t$ ($\mu$C/s) | $\delta Q_P$ (nC) | $Q$ (C) | Temp. $T_{Avg.}$ (°C) |
|---|---|---|---|---|---|---|---|---|---|---|
| 1 | Ta | 100 | 3 | 0.40 | 3.7 | 0.07 | 5.4 | 20 | 0.107 | 516 |
| 2 | | | 10 | 1.10 | 5.0 | 0.27 | 11. | 55 | 0.420 | 516 |
| 3 | Ti6Al4V-ELI | 500 | 10 | 1.10 | 5.0 | 0.38 | 11. | 55 | 0.147 | 862 |
| 4 | Ti6Al4V-ELI | 750 | 10 | 0.50 | 7.1 | 0.17 | 3.5 | 25 | 0.063 | — |
| 5 | | | | 1.00 | 10. | 0.38 | 5.0 | 50 | 0.144 | — |
| 6 | Ti6Al4V-Gr5 | 500 | 14 | 0.50 | 7.1 | 0.18 | 3.5 | 25 | 0.070 | 274 |
| 7 | | | | 1.00 | 10. | 0.40 | 5.0 | 50 | 0.153 | 392 |
| 8 | Ti6Al4V-Gr5 | 750 | 14 | 0.50 | 10. | 0.50 | 2.5 | 25 | 0.191 | 253 |
| 9 | W | 100 | 3 | 0.40 | 3.7 | 0.07 | 5.4 | 20 | 0.117 | 257 |
| 10 | | | 10 | 1.10 | 5.0 | 0.23 | 11. | 55 | 0.360 | 428 |

movable flange supplying six signal feedthroughs. Three samples are equipped with temperature sensors made of 300 $\mu$m diameter K-type thermocouples and held in place with a washer and screw.

Positron source candidate materials of different composition ($A$), thickness ($t_A$), and width ($w_A$) have been exposed to the electron beam: titanium alloys, pure tantalum, and pure tungsten (Table 1). Both the ILC [6, 11] and Ce$^+$BAF [12] positron targets imagine a rotating rim which is water-cooled (Ce$^+$BAF) or cooled by thermal radiation (ILC). Accordingly, the operation of the target can be characterized by an average temperature $T_{Avg.}$ and a temperature increase $\Delta T$ each time the same area is exposed to beam. Correspondingly, a material irradiation strategy [15] has been undertaken to mimic the expected operating conditions of the positron targets in terms of $T_{Avg.}$, $\Delta T$, and radiation damages. This was achieved using the MAMI 3.5 MeV electron beam in pulsed mode with different pulse length ($\Delta l$), period ($L$), and exposure duration (Table 1) at a 50 $\mu$A peak current from which the charge rate ($\delta Q/\delta t$), the charge per pulse ($\delta Q_p$), and the total accumulated charge ($Q$) are deduced.

Radiation damages (Table 1) are expressed in units of displacement-per-atom (dpa) and have been evaluated with FLUKA [16, 17] using the simplified [18] and improved Athermal-Recombination-Corrected [19] models. The MAMI electron beam with a 50 $\mu$m spot size and 22% duty factor radiating W-samples for ~9 h results in a damage of ~0.2 dpa, which is the expected damage of the Ce$^+$BAF tungsten target after one year of operation [5].

The temperature signals were recorded using an EX1401 acquisition system allowing to sample signals every 50 $\mu$s [20]. The $T_{Avg.}$ temperatures have been determined at the beam spot location from ANSYS [21] simulations with a 50 $\mu$m spot width and the heat load corresponding to the different pulse schemes (Fig. 1). Measurements performed at a distance from the beam spot are consistent with ANSYS evaluations. That distance further leads to a strong decrease of the cycling temperature rise: from simulations, $\Delta T$ is damped within a <1 mm distance. In this case, the mechanics holding the thermocouples occupies a 4 mm diameter area, which makes difficult the experimental access to $\Delta T$. A typical measurement during irradiation shows an average temperature together with a temperature rise at each pulse, $\widetilde{T}_{Avg.}$=762°C and $\Delta\widetilde{T}$=1.5°C in the example of

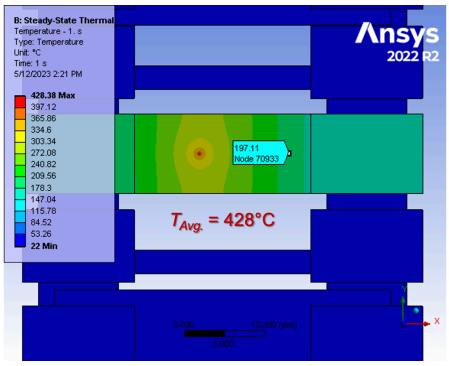


Figure 1: ANSYS simulation of W-sample #10 temperature during irradiation showing the average temperature at the beam spot and the one at the thermocouple location.

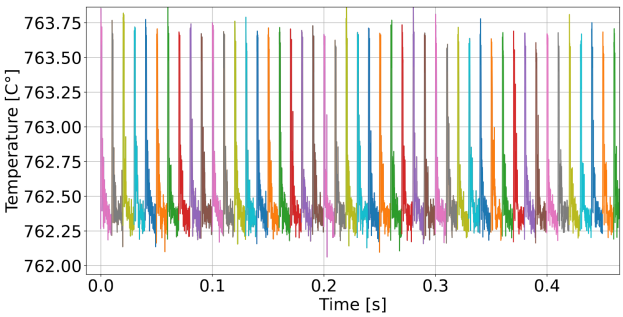


Figure 2: Cycling measurement of a Ti6Al4V-ELI sample.

(Fig. 2). While it is remarkable to observe a pulse effect, this measurement is not relevant of the sample behaviour because the beam was found to also be located on the thermocouple holder. This measurement was consequently excluded of the final analysis. Those of Table 1 do not observe sizeable cycling effects because of the distance to the beam spot.

## DAMAGES CHARACTERIZATION

The sample structure was investigated in transmission geometry using the high penetration power of the high energy X-ray radiation provided by the HEMS beamline at PETRA-III (DESY) operated by the Helmholtz-Zentrum Hereon. The bright beam can be focused to only tens of $\mu$m$^2$ enabling precise mapping of the samples in a destruction free way. With a photon energy of 87.1 keV the short acquisition time for each diffraction pattern allows characterization of a large area in and around the beam spot. The scattered beam was recorded with a two-dimensional (2D) detector and the resulting diffractograms analyzed in the relevant areas. Subsequently, they were reduced to one-dimensional (1D) patterns via radial integration to obtain more quantitative information on the structure changes from a detailed analysis of multiple diffraction peaks. These were compared to results from never irradiated witness samples made of exactly the same material.

The analysis of 2D-diffractograms distinguishes W-sample #10 as the most damaged sample of the study, as

ISBN: 978-3-95450-247-9 ISSN: 2673-5490 doi: 10.18429/JACoW-IPAC2024-TUPC81



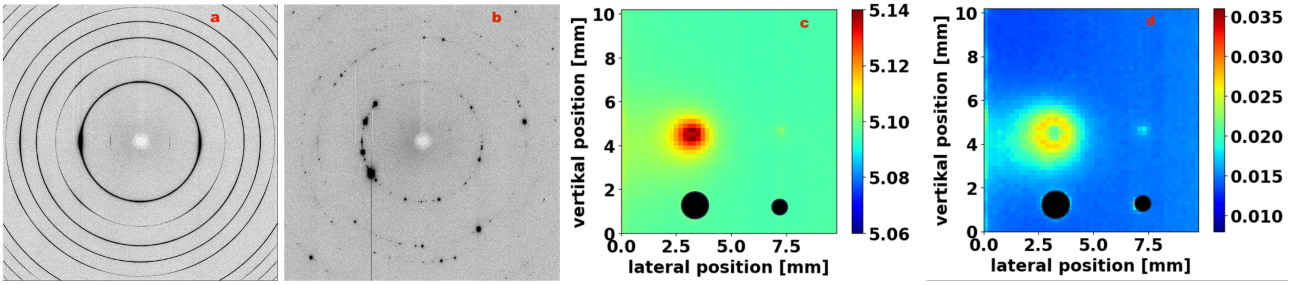


Figure 3: Example of radiation damage diagnostics: diffraction pattern of the W-sample #10 outside (a) and inside (b) the irradiated area; map of the scattering angle (c) and peak width (d) resulting from the peak analysis of the $\beta$-phase of the titanium sample #5, where black circles indicate the location of two alignment holes.

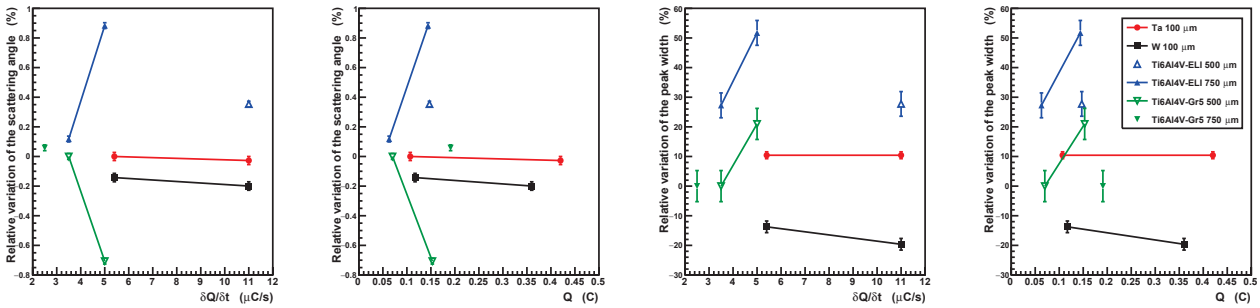


Figure 4: Relative variations of the scattering angle (left plots) and of the peak width (right plots) as function of the charge rate $\delta Q/\delta t$ and the total accumulated charge $Q$; the different samples are distinguished by different symbols. For the titanium alloys the results for the $\beta$-phase of titanium were used.

observed on the diffractograms of Fig. 3 showing a significant change of the grain size. The effect even extends over an area larger than the beam spot size. This questionable observation may result from an uncontrolled overheating event and should be confirmed in future measurements. The other samples did not show such change of the grain size: Ti6Al4V alloys exhibit small changes only at the beam spot, and no change at all was observed for Ta, even for sample #2 with the same charge rate and larger exposure time than W.

The analysis of 1D-patterns provides a finer view of structural modifications in terms of the changes of the scattering angle and peak width relative to witness samples (Fig. 4). W-samples show modifications of the scattering angle and peak width even for the smallest charge rates tested. These changes extend to an area larger than the size of the beam spot. For Ta-samples the peak parameters shifted in the entire sample relative to the reference value, but no further changes could be observed at the beam spot. Both the $\alpha$- and $\beta$-phase of Ti6Al4V alloys were studied. Changes for both phases are observed at high charge rates. The changes in the $\beta$-phase (Fig. 4) were more prominent and started at lower charge rates. Notably, Gr5 and ELI variants behave differently with respect to the scattering angle modifications. For the most intense irradiation the largest increase in the peak width occurs at the edge of the beam spots and not along the path of the electron beam.

The changes observed in the peak parameters for Ti6Al4V alloys of the present study appear correlated with the charge rate. For the Ti Gr5 samples these changes do not align with changes observed in similar samples uniformly heated inside an oven [22, 23]. The decrease in the lattice parameter and therefore increase in scattering angle is in stark contrast with the one from heating the alloy to a higher temperature.

## CONCLUSION

Measurements presented in this work are a first indication of the radiation hardness behaviour of different materials considered for positron production. While Ti6Al4V alloys and W appear strongly sensitive to irradiation, the relative absence of damages for Ta is unexpected and unexplained. However, measurements distinguishing the correlation between radiation and temperature effects, and their dependence on the accumulated charge, was limited. A new measurement campaign will revisit these observations with an experimental set-up upgraded for accurate determination of the beam size, advanced control and knowledge of its position, and better temperature measurements. The confirmation of the Ta-sample behaviour would definitely open new avenues for positron source materials.

## ACKNOWLEDGEMENTS

We thank the colleagues of the mechanical and vacuum workshops for their critical help and active participation during the installation of the target holder, and the MAMI operators for providing stable and reproducible electron beam.

ISBN: 978-3-95450-247-9 ISSN: 2673-5490 doi: 10.18429/JACoW-IPAC2024-TUPC81

# REFERENCES


[1] G. Moortgat-Pick *et al.*, "The role of polarized positrons and electrons in revealing fundamental interactions at the linear collider," *Phys. Rept.*, vol. 460, pp. 131–243, 2008. doi:10.1016/j.physrep.2007.12.003

[2] K. Fujii *et al.*, "The role of positron polarization for the inital 250 GeV stage of the International Linear Collider," 2018. doi:10.48550/arXiv.1801.02840

[3] A. Accardi *et al.*, "An experimental program with high duty-cycle polarized and unpolarized positron beams at Jefferson Lab," *Eur. Phys. J. A*, vol. 57, no. 8, p. 261, 2021. doi:10.1140/epja/s10050-021-00564-y

[4] P. Musumeci *et al.*, "Positron sources for future high energy physics colliders," 2022. doi:10.48550/arXiv.2204.13245

[5] A. Ushakov, S. Covrig, J. Grames, S. Habet, C. Le Galliard, and E. Voutier, "Evaluation of a high-power target design for positron production at CEBAF," in *Proc. 14th International Particle Accelerator Conference (IPAC'23)*, 2023, pp. 3842–3844. doi:10.18429/JACoW-IPAC2023-WEPM120

[6] S. Riemann, P. Sievers, G. Moortgat-Pick, and A. Ushakov, "Updated status of the undulator-based ILC positron source," in *International Workshop on Future Linear Colliders (LCWS2020)*, 2020. doi:10.48550/arXiv.2002.10919

[7] A. Mikhailichenko *et al.*, "The E166 experiment: Undulator-based production of polarized positrons," *AIP Conf. Proc.*, vol. 915, no. 1, pp. 1095–1100, 2007. doi:10.1063/1.2750960

[8] G. Alexander *et al.*, "Observation of Polarized Positrons from an Undulator-Based Source," *Phys. Rev. Lett.*, vol. 100, p. 210 801, 2008. doi:10.1103/PhysRevLett.100.210801

[9] G. Alexander *et al.*, "Undulator-Based Production of Polarized Positrons," *Nucl. Instrum. Meth. A*, vol. 610, pp. 451–487, 2009. doi:10.1016/j.nima.2009.07.091

[10] V. E. Balakin and A. A. Mikhailichenko, "The conversion system for obtaining high polarized electrons and positrons," Budker INP, Tech. Rep. 79-85, 1979.

[11] H. Nagoshi *et al.*, "A design of an electron driven positron source for the internationallinear collider," *Nucl. Instrum. Meth. A*, vol. 953, p. 163 134, 2020. doi:10.1016/j.nima.2019.163134

[12] J. Grames *et al.*, "Positron beams at Ce+BAF," in *Proc. 14th International Particle Accelerator Conference (IPAC'23)*, 2023, pp. 896–899. doi:10.18429/JACoW-IPAC2023-MOPL152

[13] D. Abbott *et al.*, "Production of Highly Polarized Positrons Using Polarized Electrons at MeV Energies," *Phys. Rev. Lett.*, vol. 116, no. 21, p. 214 801, 2016. doi:10.1103/PhysRevLett.116.214801

[14] P. Heil *et al.*, "High energy density irradiation with MAMI linac," in *Proc. 8th International Particle Accelerator Conference (IPAC'17)*, 2017, pp. 1296–1299. doi:10.18429/JACoW-IPAC2017-TUPAB003

[15] A. Ushakov *et al.*, "Material tests for the ILC positron source," in *Proc. 8th International Particle Accelerator Conference (IPAC'17)*, 2017, pp. 1293–1295. doi:10.18429/JACoW-IPAC2017-TUPAB002

[16] C. Ahdida *et al.*, "New capabilities of the FLUKA multi-purpose code," *Frontiers in Physics*, vol. 9, paper 788253, 2022. doi:10.3389/fphy.2021.788253

[17] G. Battistoni *et al.*, "Overview of the FLUKA code," *Annals of Nuclear Energy*, vol. 82, pp. 10–18, 2015. doi:10.1016/j.anucene.2014.11.007

[18] A. Fasso, A. Ferrari, G. Smirnov, F. Sommerer, and V. Vlachoudis, "Fluka realistic modeling of radiation induced damage," *Progress in Nuclear Science and Technology*, vol. 2, pp. 769–775, 2011. doi:10.15669/pnst.2.769

[19] K. Nordlund *et al.*, "Improving atomic displacement and replacement calculations with physically realistic damage models," *Nature Communications*, vol. 9, pp. 1–8, 2018. doi:10.1038/s41467-018-03415-5

[20] VTI Instruments, https://www.vtiinstruments.com

[21] ANSYS, https://www.ansys.com/

[22] T. Lengler, D. Lott, G. Moortgat-Pick, and S. Riemann, "Target tests for the ILC positron source," in *International Workshop on Future Linear Colliders (LCWS2023)*, 2023. doi:10.48550/arXiv.2308.15916

[23] T. Lengler, "Untersuchung von strukturänderungen in Ti-6Al-4V mittels hochenergetischer Röntgenstrahlung verursacht durch schnelles zyklisches heizen," Master Thesis, Univer-sität Hamburg, 2022.